Theoretical Prediction of Roll Moment on Wing-Controlled Missile

Sadao Akishita*
Mitsubishi Electric Corporation, Amagasaki, Japan
Ryujiro Kurosaki†
Mitsubishi Electric Corporation, Kamakura, Japan
and
Kanzo Okada‡ and Tomoji Hirata§
Mitsubishi Research Institute Inc., Tokyo, Japan

A computational scheme capable of making an accurate prediction of roll moment for a wing-control configuration is presented. The panel method is employed to solve the subsonic potential flow. The trailing vortex sheet shed from the wing is modeled by a bundle of vortex filaments, and the distortion of the vortex sheet is determined by coupling the panel method with an iterative technique. Calculated roll moment for the wing-control configuration of in-line tail arrangement is compared with the measured data, and satisfactory agreement between them is obtained. Since the adopted scheme has been proven accurate, it is applied to investigate the effects of missile configurations of the roll moment. This investigation focuses on the following: 1) the problem of the roll moment of the interdigitated tail arrangement, and 2) an analysis of the effect of tail span ratio to the adverse roll moment induced upon tail surfaces.

Introduction

A WING-CONTROL configuration consisting of forward wings and tails is used in many types of guided missiles because of its fast aerodynamic response and the advantageous location of servo mechanisms.[1] However, several flaws associated with wing-control configurations must be carefully considered at the design stage. The most severe of these is roll controllability. Free-wake vortices shed downstream from deflected wings induce an adverse roll moment on tail surfaces. The roll control moment generated on the wings is, in some cases, completely canceled out by the adverse moment, and thus roll stabilization by the wing-control configuration is not achieved. In order to predict the roll moment of the configuration, the distortion of the trailing vortex sheet should be calculated as precisely as the pressure distribution on the wing surfaces and the vorticity distribution on the sheet. In the simplest procedure, the free-wake vortices are represented by an integrated vortex filament of a straight line whose location is assumed, and the induced lift on a tail surfaces is obtained.[2] Shinar[3] and Gur et al.[4] extended this procedure for canard-control configurations at supersonic range within small angles of attack. Recent advances in computer software and hardware make it easy to model a more realistic flow. Dillenius et al.[5] have developed the missile aerodynamics prediction programs that include methods to account for the effects of forward fin wakes on the afterbody and tail fins. Their results of the roll moment computation at supersonic range were compared rather satisfactorily with the experimental data. Recently, we have developed the missile aerodynamics prediction program[9] of subsonic range applying the panel method of subsonic potential flow. The program is applied in predicting the roll moment of a wing-body-tail configuration. Within a range of not large angles of flow incidence or wing deflection, the flow separation does not occur; thus modeling of potential flow can be regarded as adequate. Free-wake vortices shed from deflected wings are transformed into several vortex filaments. In other words, the distortion of the trailing vortex sheet can be represented by that of vortex filaments. The location of a wake vortex filament can be determined by an iterative procedure satisfying the boundary condition of solid surfaces for each onset of flow.[7] Some improvements to accelerate the rate of convergence are made in determining the location of the vortex filament. The results of calculation are compared with data taken from Sekaran's experiment[8] for the wing-control configuration, and the agreement is satisfactory within the range of moderate angles of flow incidence. Then two topics concerning the configuration design are addressed. One of them is the comparison between an in-line tail configuration and an interdigitated one; the other is the effect of the span ratio of tail to wing.

Presented as Paper 84-2148 at the AIAA Applied Aerodynamics Conference, Seattle, WA, Aug. 21-23, 1984; received Jan. 5, 1985; revision received April 21, 1986.

*Research Scientist, Central Research Laboratory. Member AIAA.
†Aerodynamics Engineer, Kamakura Works.
‡Staff Researcher.
§Senior Staff Researcher.

Calculation Model Description

The configuration shown in Fig. 1 is adopted as a typical model of a wing-control missile. The streamwise cross section of wings and tails are both of diamond shape. This choice, being identical to that employed in Sekaran's experiment,[8] will facilitate an appropriate comparison between the results of our calculation and the experiment.

Calculation Procedure

Solution Method

An inviscid, irrotational, compressible, steady flow is assumed. Applying the approximation of linearity, the elliptic-type partial differential equation of perturbation velocity potential is derived for a subsonic flow. This equation can be reduced to the Laplace equation of the velocity potential with the aid of the coordinate transformation. This means that any subsonic compressible flow can be reduced to the corresponding incompressible flow within a limit of the linealization approximation. In the following, only an incompressible flow is discussed, and this reduction of the problem is convenient in the comparison of the results of our calculation and Sekaran's experiment.

Our solution method is based on Morino et al.,[6] and the details of the method are neglected in the following. The basic equation is the integral equation of the velocity potential on a body surface,

$$2\pi\phi(P) - \iint_{S_A} \phi(Q)\frac{\partial}{\partial n(Q)}\left[\frac{1}{R}\right]dS - \iint_{S_W} \Delta\phi(Q)\frac{\partial}{\partial n(Q)}\left[\frac{1}{R}\right]dS = \iint_{S_A} U_\infty \cdot n(Q)\left[\frac{1}{R}\right]dS \quad (1)$$

where the frame of reference is defined, as shown in Fig. 2, such that the x axis is parallel to the undisturbed uniform flow velocity U_∞ and inclined to the body axis by an angle α. In the figure, P is an observation point on a body surface S_A; S_W the wake vortex sheet which emanates from the trailing edge C_W, Q an evaluation point in integrating on the surfaces; R the distance between P and Q; and n an outward normal unit vector. In Eq. (1), $\Delta\phi$ is the potential jump across the sheet given in accordance with the Kutta condition and $\iint$ means taking the principal value of the integral where $R=0$.

In order to obtain a numerical solution of Eq. (1), the body surface S_A and the wake vortex sheet S_W are divided into quadrilateral panel elements Σ_k and Σ_k', respectively. In each of the body surface elements, ϕ is represented by its value at the centroid P_k of the element. The collocation method is applied, in which Eq. (1) is made compatible at a centroid $P_{k=h}$ of each element Σ_k. This yields

$$[\delta_{hk} - C_{hk} - W_{hk}]\{\phi_k\} = [b_{hk}]\{U_\infty \cdot n_k\} \quad (2)$$

$$(h,k = 1,2,\ldots,m)$$

where the summation rule for k is preserved, and δ_{hk} is Kronecker's delta and m the number of the body surface elements. C_{hk}, b_{hk}, and W_{hk} are the influence coefficients defined by the following equations:

$$C_{hk} = \frac{1}{2\pi}\left[\iint_{\Sigma_k} \frac{\partial}{\partial n}\left(\frac{1}{R}\right)dS\right]_{P=P_h} \quad (3a)$$

$$b_{hk} = \frac{1}{2\pi}\left[\iint_{\Sigma_k} \frac{1}{R}dS\right]_{P=P_h} \quad (3b)$$

$$W_{hk} = \pm\frac{1}{2\pi}\left[\iint_{\Sigma_k'} \frac{\partial}{\partial n}\left(\frac{1}{R}\right)dS\right]_{P=P_h} \quad (3c)$$

C_{hk} and b_{hk} are evaluated by taking the principal value of the integral where $h=k$. W_{hk} is evaluated only for the elements Σ_k that are in contact with the trailing edge and summing up the contributions from all the elements comprising a wake vortex sheet $\Sigma_{k'}$. The upper (lower) sign in front of the integral for W_{hk} must be used for the upper (lower) side of the wake sheet. The flowfield ϕ is obtained by solving the linearized Eq. (2). Once the value of ϕ on the body surface is determined, the flow velocity $V(P_h)$ is computed by the following:

$$V(P_h) = [C_{hk} + W_{hk}]\{\phi_k\} + [b_{hk}]\{U_\infty \cdot n_k\} \quad (4)$$

where

$$C_{hk} = \{\text{grad}(C_{hk})\}_{P=P_h} \quad (5a)$$

$$W_{hk} = \{\text{grad}(W_{hk})\}_{P=P_h} \quad (5b)$$

$$b_{hk} = \{\text{grad}(b_{hk})\}_{P=P_h} \quad (5c)$$

The pressure distribution is obtained from the resultant velocity $V(P_h)$ and U_∞ by applying Bernoulli's theorem.

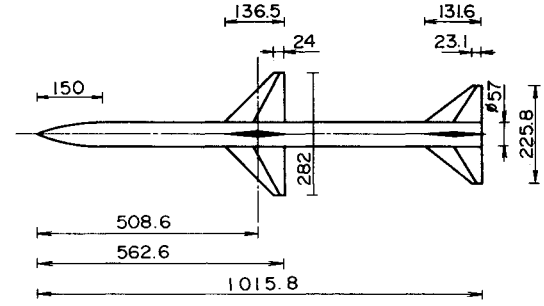

Fig. 1 Schematics of wing-controlled missile configuration.

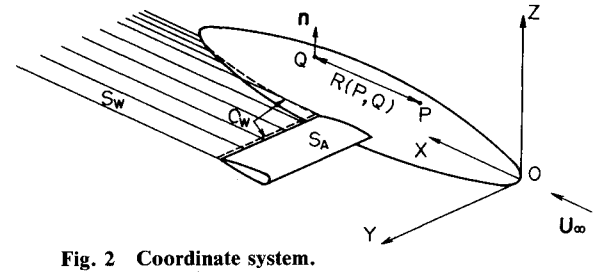

Fig. 2 Coordinate system.

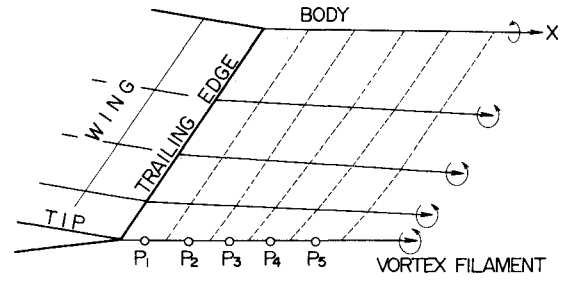

Fig. 3 Trailing vortex sheet modeling.

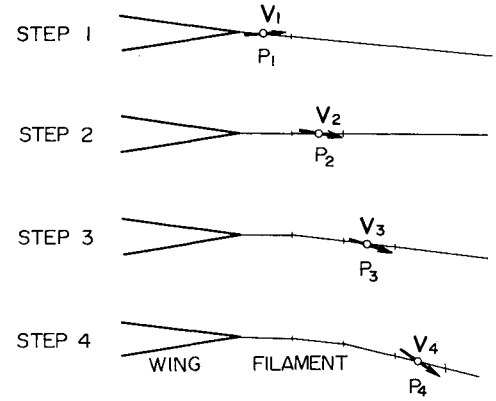

Fig. 4 Modification of line segment location.

Location of a Trailing Vortex Sheet

A trailing vortex sheet is represented by a potential jump $\Delta\phi$ which is constant over the sheet, and the potential jump is equivalent to a constantly distributed doublet sheet. In the potential flow theory, a constantly distributed sheet is replaceable by a closed vortex sheet filament ring surrounding the sheet. In our case, a trailing vortex sheet emanates from only a wing trailing edge. When the wing surface is divided into n streamwise column panels on the upper and lower side (in Figs. 3 and 7a, $n=4$), the trailing vortex sheet is composed of n semi-infinite sheets in which constant strength doublets

are distributed respectively. Thus, the trailing vortex sheet can be modeled by a set of $n+1$ discrete vortex filaments as shown in Fig. 3. The vortex filament must run along the local flow direction. Since a vortex filament has been divided into line segments in this study, each segment must be located so as to run in parallel with a local flow vector. When the starting point (x_j, y_j, z_j) of the line segment is given, a terminal point $(x_{j+1}, y_{j+1}, z_{j+1})$ is determined as follows:

$$y_{j+1} = \left[\frac{U_{\infty_y} + v_y}{U_{\infty_x} + v_x}\right]_{P=Pj} (x_{j+1} - x_j) + x_j \qquad (6a)$$

$$z_{j+1} = \left[\frac{U_{\infty_y} + v_z}{U_{\infty_x} + v_x}\right]_{P=Pj} (x_{j+1} - x_j) + z_j \qquad (6b)$$

where the x coordinate is assigned and fixed.

In the panel method, all locations of the sources and doublets must be specified when the governing Eq. (2) is applied to determine their strength. The locations of the body surface elements may be fixed throughout all stages of the composition. However, since the initial locations of the vortex filaments cannot be specified, they must be assigned arbitrarily at the initial state. In this study, the vortex filaments are assumed to be a straight, semi-infinite line running almost along U_∞ vector but not intersecting the body or the wings. After the strength of all sources and doublets on the body surface elements is determined, the strength $\Delta\phi$ of the doublets on the wake vortex sheets can be specified in accordance with the Kutta condition of the trailing edge of the wing. Then, all (n) wake sheets are divided into quadrilateral panel elements of which two streamwise sides are identified with the line segments of the vortex filaments as shown in Fig. 3. Then relocation of the vortex filaments is done on every center point of the line segments using Eqs. (6a) and (6b). The flow velocity vector (v_x, v_y, v_z) is calculated with the above-mentioned strength of sources and doublets using Eq. (4) at $P=P_j$. At this stage, the technique shown in Fig. 4 is efficient at accelerating the rate of convergence of the line segment location. When the vortex filament line segments are modified from the upstream-most segment, adjacent to the trailing edge, the vortex filament is assumed to be a straight, semi-infinite line (step 1). In the calculation of the direction of the next segment, the downstream segments are assumed to be straight and parallel to the direction of the element just upstream (step 2). The very same procedure is repeated for the rest of the line segments (step 3 and step 4). These procedures are approximate ones because the downstream segments generally are not straight. But the error resulting from the assumption is small and permissible for the economy of computation time. At the next stage, we calculate again the strength of all sources and doublets with the relocated wake vortex filaments. This process is iterated until the discrepancies are sufficiently small.

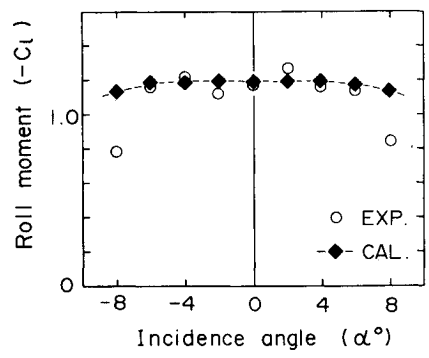

Fig. 5 Roll moment variation of the tail-off configuration for horizontal wing deflection, $\delta = 4$ deg.

Results and Discussion

Comparison Between Calculation and Experiment

The computational results obtained in the present work are shown compared with the corresponding experimental results performed by Sekaran.[8] The control-wing deflection angle δ is fixed at 4 deg. In Fig. 5, roll moment variation of the tail-off configuration for horizontal wing deflection is shown. In Fig. 5 and in the following roll moment, C_l is defined as follows:

$$C_l = \frac{\ell}{(\pi/4) D_b^3 \cdot q_\infty} \qquad (7)$$

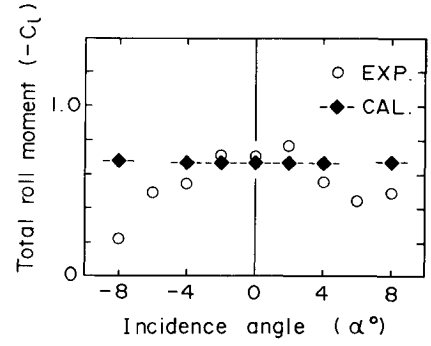

Fig. 6 Roll moment variation of the total body configuration for horizontal wing deflection; in-line tail arrangement, $\delta = 4$ deg.

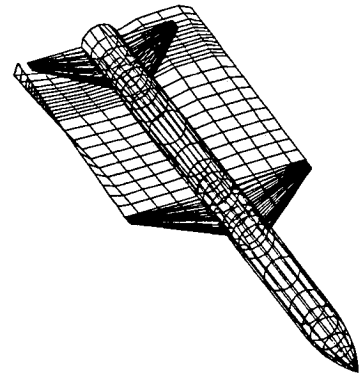

Fig. 7a Panel division of the missile and the trailing vortex sheet for horizontal wing deflection, $\delta = 4$ deg, $\alpha = 4$ deg.

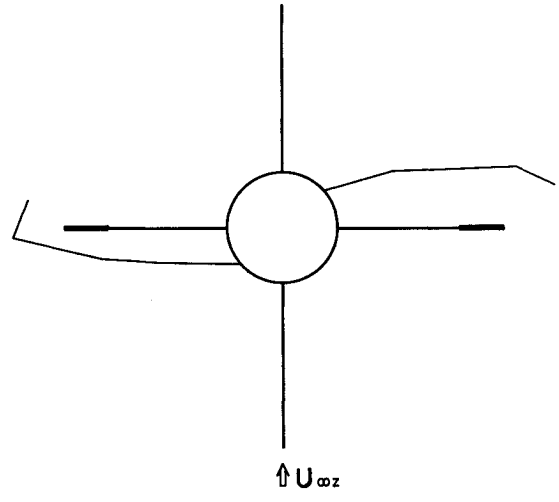

Fig. 7b Cross-sectional view of the trailing vortex sheet at aft end of the body; horizontal wing deflection $\delta = 4$ deg, $\alpha = 4$ deg.

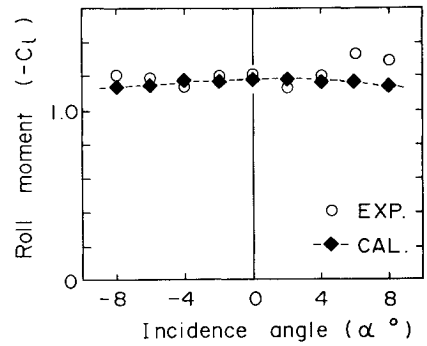

Fig. 8 Roll moment variation of the tail-off configuration for vertical wing deflection, $\alpha = 4$ deg.

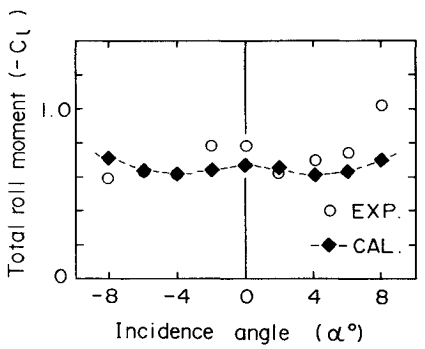

Fig. 9 Roll moment variation of the total body configuration for vertical wing deflection; in-line tail arrangement, $\delta = 4$ deg.

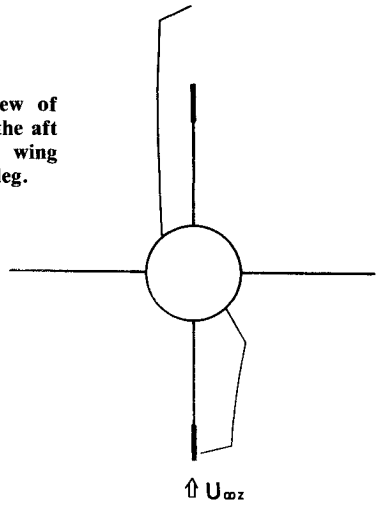

Fig. 10 Cross-sectional view of the trailing vortex sheet at the aft end of the body; vertical wing deflection, $\delta = 4$ deg, $\alpha = 4$ deg.

where ℓ is roll moment around the x axis, D_b the diameter of the body, and q_∞ the dynamic pressure of the flow. The calculated results agree well with the experiment, within a reasonable degree of accuracy in a range of $|\alpha| \leq 6$ deg. The roll moment of the total body configuration for horizontal wing deflection is shown in Fig. 6. In this case the tails are arranged in-line with the wings. The agreement between the calculation and the experiment is satisfactory at a range of $|\alpha| \leq 4$ deg, but poor at $|\alpha| = 8$ deg. This difference seems to be inevitable, since that of the tail-off configuration becomes considerable at the same incidence angle (see Fig. 5). The calculated results are dropped at $|\alpha| = 6$ deg; the reason for this is explained below. Figure 7a shows the panel division of the total body (1174 panels) and the distortion of the trailing vortex sheets (176 panels) at $\alpha = 4$ deg, while Fig. 7b shows the cross-sectional view of the vortex sheet at the aft end of the body. The vortex filament at the innermost position is attached to the body surface. The innermost filament of a straight line is identified with the side of the body panel elements. Therefore, if the location of the filament is corrected at every iteration, the body panels must also be rearranged accordingly. In our analysis, the innermost filament is fixed at the initial position for the economy of computing time, since the circulation of the filament and its influence on the induced moment is minimal. This approximation was justified by the following fact. The difference in the roll moments between two cases, where the locations of the innermost filaments differ considerably, is negligibly small, and the locations of other outer filaments converge to the same positions, respectively. In Fig. 7b the wings are deflected to generate a clockwise roll moment. The trailing edge of the horizontal left wing is moved down and that of the horizontal right wing is moved up. The left innermost filament emanating from the trailing edge of the left wing runs along the lower surface of the body, and the right innermost filament from the trailing edge of the right wing runs along the upper surface of the body. Then the left trailing vortex sheet stems from the lower position of the body and the right one stems from the upper position. Since $\alpha > 0$, the incident flow washes upward and the outer parts of the sheets moved upward. The contributions of all wings and tails to the total roll moment are shown in Table 1, where it is found that all panels, except the horizontal control wings, contribute to the reversed roll moment. The compositions of induced roll moment on the tails are shown in Table 2. The induced roll moment on the tails amounts to about 40% of the total moment on the wings. Computation time for a typical incidence angle is about 20 min with an IBM 3081.

It is also possible for the trailing vortex sheet shed from the wing to go through the tail. In Fig. 6, at $\alpha = 0 \sim 4$ deg, the left vortex sheet goes below the tail as shown in Fig. 7b, and at $\alpha = 8$ deg it goes above the tail. At $\alpha = 6$ deg, the inner three vortex filaments go below the tail, while the outer two go above the tail. Thus the vortex sheet intersects the tail between

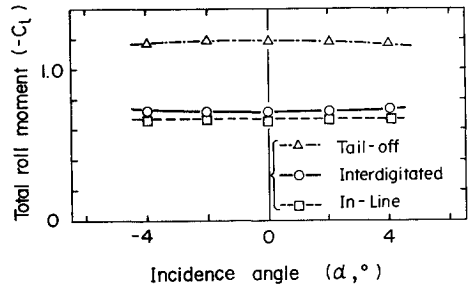

Fig. 11 Comparison of the computed roll moment between the interdigitated and in-line arrangement, $\delta = 4$ deg.

Table 1 Contributions of roll moment of total body configuration for horizontal wing deflection; in-line tail arrangement, $\delta = 4$ deg, $\alpha = 0$ deg

$-C_{l\ \text{control wings}}$	1.623
$-C_{l\ \text{vertical wings}}$	−0.438
$-C_{l\ \text{tails}}$	−0.528
$-C_{l\ \text{total}}$	0.662

Table 2 Compositions of induced roll moment on tails for horizontal wing deflection; in-line tail arrangement, $\delta = 4$ deg

α	0 deg	2 deg	4 deg
$-C_{l\ \text{total}}$	0.662	0.663	0.669
$\Delta C_{l\ \text{induced horizontal}}$	−0.525	−0.525	0.516
$\Delta C_{l\ \text{induced vertical}}$	−0.003	0.002	0.006

the third and the fourth filament. Singularity of the flow on the tail surfaces can be avoided where a new division of the surface panels is added on the intersecting lines. We did not succeed in trying this new algorithm, since convergence of the location of the intersecting lines was not realized. This is the reason the calculated results of $\alpha = \pm 6$ deg are dropped in Fig. 6.

Pitch control of a missile is assigned to the horizontal wings, and in some cases roll control is assigned to the vertical wings to decouple the control functions. Figure 8 shows the roll moment variation of the tail-off configuration and for the vertical wing deflection. Reasonable agreement between the calculation and the experiment is obtained. The tails are arranged in-line with wings in this case. Agreement between the calculation and the experiment is moderate, except at $\alpha = 8$ deg. Discrepancies between these two at $\alpha = -2$ and 0 deg seem to be not due to the calculation. In spite of the identical configuration and flow condition at $\alpha = 0$ deg, the experimental results differ rather noticeably, as shown in Figs. 6 and 9. On the other hand, the calculated result of the roll moment for the case of vertical wing deflection is identical with that for the case of horizontal wing deflection. Of course, the difference between the vertical and the horizontal wing increases with $|\alpha|$ value. Figure 10 shows a cross-sectional view of the trailing vortex sheet for vertical wing deflection at the aft end of the body. As shown in the figure, the outer tip of the lower sheet is very close to the tail. This distortion of the vortex sheet causes a strong reversed roll moment on the tail, resulting in a larger decrease of the total moment.

Effect of Tail Arrangement on the Roll Moment

An interdigitated tail arrangement has been recommended to prevent reversed roll moment from being induced on the tail surfaces.[3] Since the trailing vortex sheets run remote from the tails in this arrangement, the reversed roll moment is expected to lessen. In Fig. 11, a comparison is made of the calculated roll moment between the interdigitated and the in-line tail arrangement. The wing and tail planform remains unchanged for both of the arrangements as shown in Fig. 1. As expected, the roll moment for the interdigitated tail arrangement is larger than that for the in-line tail arrangement. But the difference between them is not appreciable. Figure 12a shows the trailing vortex sheets for the interdigitated tail arrangement, and Fig. 12b is a cross-sectional view at the aft end of the body. In this case, the horizontal control wings are deflected. The cross-sectional view of the trailing vortex sheet in Fig. 12b differs appreciably from those for in-line tail arrangement shown in Figs. 7b and 10.

Effect of Tail Span Ratio on the Induced Roll Moment on Tails

As was mentioned, when the outer tip of the trailing vortex sheet gets close to the tip of a tail, there occurs an appreciable effect on the induced roll moment on the tail surfaces. The effect of tail span ratio on the induced roll moment on the tails is calculated for the configuration shown in Fig. 1. The original span ratio of the tail to the wing for this configuration is just 0.8. In our calculation only the tail span is varied keeping the other parts of the configuration unchanged. As similarity of the tail planform is preserved, the aspect ratio of the exposed tail part remains constant. The area of the exposed tail is proportional to the second power of $(S_T - D_b)/S_W$, where S_T and S_W mean the span of the tail and the wing, respectively. The result of the calculation is shown in Fig. 13. It is found that the induced roll moment decreases remarkably with the tail span ratio. From the viewpoint of effective roll control, it is recommended that the tail span ratio should be kept as low as possible. In the case shown in Fig. 13, the adverse roll moment induced on the tail exceeds the roll moment generated on the wings of $S_T/S_W = 1.0$. In order to preserve enough margin for the pitch stability, the tail span ratio should be larger than a threshold. This indicates that a

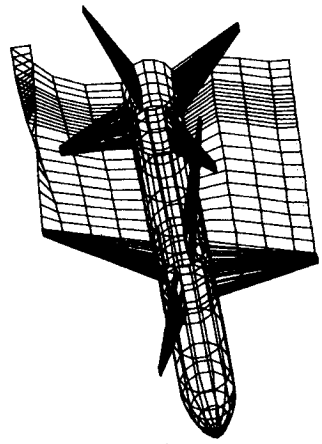

Fig. 12a Panel division of the missile and the trailing vortex sheet for the interdigitated tail arrangement, $\delta = 4$ deg, $\alpha = 4$ deg.

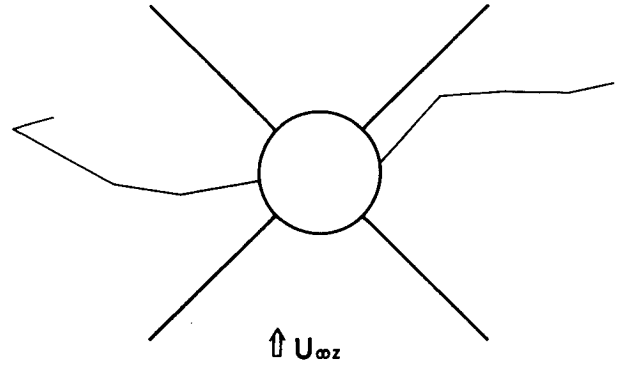

Fig. 12b Cross-sectional view of the trailing vortex sheet at the aft end of the body; interdigitated tail arrangement.

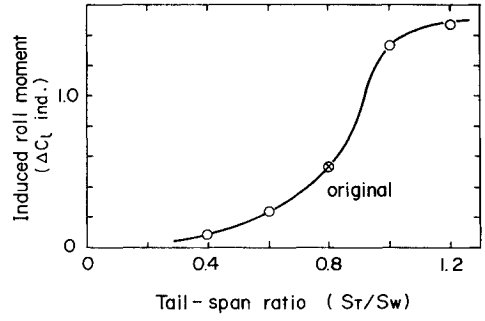

Fig. 13 Effect of the tail span ratio upon the induced roll moment on tails; in-line tail arrangement, $\delta = 4$ deg, $\alpha = 4$ deg.

missile configuration designer must often pursue a narrow range of tail span ratios where the effectiveness or roll control is compatible with the margin for the pitch stability. The calculation method presented in this paper has proven very efficient for predicting the roll controllability.

Conclusion

A computational scheme capable of making an accurate prediction of roll moment for a wing-controlled missile at subsonic range was presented. The panel method solution of potential flow was obtained and extended to calculate the distortion of the trailing vortex sheet and the roll moment induced on the tail surfaces. The results of the roll moment calculation were compared with Sekaran's experimental data, yielding the satisfactory agreements about horizontal and vertical wing deflection for tails in-line with wings. The effect of tail arrangement to roll moment was calculated. It was also found that the roll moment for the interdigitated arrangement of the wings and tails were slightly larger than that for the in-line arrangement. The effect of tail span ratio on the roll mo-

ment was evaluated by varying only the tail span and keeping the other parts of the configuration unchanged. As a result, it was found that the adverse roll moment induced on the tails decreased remarkably with the tail span ratio. Thus, it may be concluded that the span ratio should be kept as low as possible in order to acquire an effective roll control.

References

[1]Chin, S.S., *Missile Configuration Design,* McGraw-Hill Book Co., New York, 1961.

[2]Nielsen, J.N., *Missile Aerodynamics,* McGraw-Hill Book Co., New York, 1960.

[3]Shinar, J., "Roll Control Feasibility of Slender Cruciform Configuration by Canard Surfaces at Mach Number 2.25," *Israel Journal of Technology,* Vol. 12, 1974, pp. 31–39.

[4]Gur, I., Shinar, J., and Rom, J., "Prediction of Roll Controllability of Slender Cruciform Canard Configurations," *Journal of Spacecraft and Rocket,* Vol. 16, July-Aug. 1979, pp. 238–244.

[5]Dillenius, M.F.E., Hemsch, M.J., Sawyer, W.C., Allen, J.M., and Blair, A.B. Jr., "Comprehensive Missile Aerodynamics Programs for Preliminary Design, *Journal of Spacecraft and Rockets,* Vol. 20, Aug. 1983, pp. 414–416.

[6]Morino, L., Chem, L.T., and Suciu, E.O., "Steady and Oscillatory Subsonic and Supersonic Aerodynamics around Complex Configurations," *AIAA Journal,* Vol. 13, March 1975, pp. 368–374.

[7]Laubrujere, Th.E. and Sytsma, H.A., "Aerodynamic Interference between Aircraft Components: The Possibility of Prediction," ICAS Paper No. 72-49, Aug. 1972.

[8]Sekaran, V.G., "Subsonic Rolling Moment for Wing Roll Control of a Cruciform Missile Model," *Journal of Spacecraft and Rockets,* Vol. 20, March-April 1983, pp. 97–98.

[9]Akishita, S., Kurosaki, R., and Katayama, M., "Development of a Computational Aerodynamics Program (SUSCAP) for Missile Configuration Design," *Mitsubishi Denki Giho,* Vol. 59, 1985, pp. 42–46 (in Japanese).